Ratiometric two-photon microscopy reveals attomolar copper buffering in normal and Menkes mutant cells

M. Thomas Morgan[a,b], Daisy Bourassa[a,b], Shefali Harankhedkar[a,b], Adam M. McCallum[a,b], Stephanie A. Zlatic[c], Jenifer S. Calvo[d], Gabriele Meloni[d], Victor Faundez[c], and Christoph J. Fahrni[a,b,1]

[a]School of Chemistry and Biochemistry, Georgia Institute of Technology, Atlanta, GA 30332-0400; [b]Petit Institute for Bioengineering and Bioscience, Georgia Institute of Technology, Atlanta, GA 30332-0400; [c]Department of Cell Biology, Emory University, Atlanta, GA 30322; and [d]Department of Chemistry and Biochemistry, The University of Texas at Dallas, Richardson, TX 75080-3021

Edited by Marcetta Y. Darensbourg, Texas A&M University, College Station, TX, and approved May 9, 2019 (received for review January 4, 2019)

Copper is controlled by a sophisticated network of transport and storage proteins within mammalian cells, yet its uptake and efflux occur with rapid kinetics. Present as Cu(I) within the reducing intracellular environment, the nature of this labile copper pool remains elusive. While glutathione is involved in copper homeostasis and has been assumed to buffer intracellular copper, we demonstrate with a ratiometric fluorescent indicator, crisp-17, that cytosolic Cu(I) levels are buffered to the vicinity of 1 aM, where negligible complexation by glutathione is expected. Enabled by our phosphine sulfide-stabilized phosphine (PSP) ligand design strategy, crisp-17 offers a Cu(I) dissociation constant of 8 aM, thus exceeding the binding affinities of previous synthetic Cu(I) probes by four to six orders of magnitude. Two-photon excitation microscopy with crisp-17 revealed rapid, reversible increases in intracellular Cu(I) availability upon addition of the ionophoric complex CuGTSM or the thiol-selective oxidant 2,2′-dithiodipyridine (DTDP). While the latter effect was dramatically enhanced in 3T3 cells grown in the presence of supplemental copper and in cultured Menkes mutant fibroblasts exhibiting impaired copper efflux, basal Cu(I) availability in these cells showed little difference from controls, despite large increases in total copper content. Intracellular copper is thus tightly buffered by endogenous thiol ligands with significantly higher affinity than glutathione. The dual utility of crisp-17 to detect normal intracellular buffered Cu(I) levels as well as to probe the depth of the labile copper pool in conjunction with DTDP provides a promising strategy to characterize perturbations of cellular copper homeostasis.

copper homeostasis | fluorescent probes | two-photon microscopy | glutathione | Menkes disease

Copper is an essential trace nutrient for most forms of life and plays critical roles in fundamental biological processes, including respiration, iron acquisition, and connective tissue formation (1). In mammalian cells, a complex network of membrane transporters, cytosolic metallochaperones, and storage proteins is responsible for acquiring, distributing, and regulating cellular copper levels (2). Within the reducing intracellular environment, copper is transported in its monovalent oxidation state (3), and increasing evidence suggests that cells maintain a ligand-bound but kinetically labile pool of Cu(I), which may serve as a buffer against fluctuations in external copper availability. Radiotracer studies with lymphoid cells revealed both rapid cellular uptake and efflux of copper, providing direct experimental evidence that a significant portion of the acquired cellular copper remains mobile and can dynamically exchange with the extracellular medium (4). While free aquacopper(I) is rapidly oxidized by molecular oxygen or precipitates as cuprous oxide at neutral pH, labile cellular copper is stabilized through coordination to proteins and low–molecular-weight biomolecules (5). For example, copper metallochaperones, which are responsible for trafficking Cu(I) to specific subcellular targets, stabilize Cu(I) through coordination to the sulfhydryl group of cysteine residues (6). Despite high complex stabilities with dissociation constants in the attomolar range or below (7), the exchange of Cu(I) between copper-transporting proteins is characterized by rapid kinetics, likely mediated through an associative exchange mechanism involving direct protein–protein interactions (8).

While modern microanalytical imaging techniques such as synchrotron X-ray fluorescence microscopy or secondary ion mass spectrometry are capable of visualizing the subcellular distribution of copper with submicron resolution (9), such methods cannot be employed for dynamic monitoring of live biological specimens and yield only total copper levels regardless of the kinetic availability. To this end, synthetic fluorescent probes that selectively respond to Cu(I) rank among the most promising tools for exploring the dynamics of labile copper in live cells (10–12). Provided that they possess suitable binding affinities and remain functional within the intracellular environment, such probes may engage in a dynamic exchange equilibrium with endogenous ligands to report on the thermodynamic and kinetic availability of labile Cu(I).

We recently devised a water-soluble Cu(I)-selective turn-on fluorescent probe, CTAP-3, which offers a detection limit in the subpart-per-trillion range and retains a high fluorescence contrast ratio even in the presence of lipid bilayers (13). Microinjection experiments of the brightly fluorescent probe–Cu(I) complex revealed an unexpected rapid dissipation of the fluorescence signal (see below), suggesting competitive chelation of Cu(I) by endogenous ligands. Although the identity of the ligands responsible for buffering labile cellular Cu(I) has not been fully established, glutathione (GSH) emerged early on as a candidate

Significance

Impaired copper regulation has been implicated in a range of human diseases, yet the current mechanistic understanding of intracellular copper homeostasis remains incomplete. While Cu(I)-selective synthetic fluorescent probes could shed light on copper homeostasis within living cells by dynamically reporting intracellular Cu(I) availability, the affinity range of previously employed probes was insufficient to achieve significant metallation in the presence of glutathione (GSH) at normal physiological concentrations. Employing an air-stable phosphine-based ligand design, we devised a ratiometric indicator capable of competing for Cu(I) at attomolar buffered levels. Contrary to prior assumptions, our ratiometric imaging data indicate that intracellular Cu(I) is not buffered directly by GSH but by thiol ligands of still higher affinity.

Author contributions: M.T.M., D.B., S.H., A.M.M., S.A.Z., J.S.C., G.M., V.F., and C.J.F. designed research; M.T.M., D.B., S.H., A.M.M., S.A.Z., and J.S.C. performed research; M.T.M., D.B., S.H., A.M.M., S.A.Z., J.S.C., G.M., V.F., and C.J.F. analyzed data; and M.T.M. and C.J.F. wrote the paper.

The authors declare no conflict of interest.

This article is a PNAS Direct Submission.

[1]To whom correspondence may be addressed. Email: fahrni@chemistry.gatech.edu.

This article contains supporting information online at www.pnas.org/lookup/suppl/doi:10.1073/pnas.1900172116/-/DCSupplemental.

Published online June 3, 2019.

based on chromatographic fractionation studies of cell lysates harvested under copper-supplemented growth conditions (14). More recent studies suggest that GSH plays an important role in the regulation of cellular copper uptake and homeostasis (15). For example, depletion of cellular GSH in HEK293 cells attenuated copper uptake, while exposure to elevated copper concentrations increased cellular GSH levels (16).

Despite the interplay between cellular copper levels and GSH, the mechanistic role of GSH in copper homeostasis remains unclear. On the basis of combined spectroscopic and potentiometric studies, we recently discovered that the major species formed by coordination of Cu(I) to GSH is an adamantane-like tetranuclear cluster (17). Concluding from the derived thermodynamic model, the millimolar levels of GSH normally present within cells limit aquacopper(I) concentrations to the subfemtomolar regime, three orders of magnitude lower than previously estimated (17). GSH can thus readily remove Cu(I) from its complex with CTAP-3, which has a dissociation constant of 50 pM. Although a sizable number of Cu(I)-selective synthetic fluorescent probes have been reported over the past decade (10–12), all of them coordinate Cu(I) via structurally similar chelators comprising amine and thioether donors, yielding a rather narrow range of affinities from the picomolar to high femtomolar range, which is insufficient to measure Cu(I) in the presence of normal cytosolic GSH levels. The rapid depletion of CTAP-3-bound Cu(I) by endogenous ligands underscores the need for probes with stronger Cu(I) affinities.

To overcome the limitations of conventional thioether-based Cu(I) chelators, we recently devised an alternative ligand design strategy featuring phosphine sulfide-stabilized phosphine (PSP) donor motifs (18). The electron-withdrawing phosphine sulfide substituents stabilize the central phosphine donor against oxidation while at the same time acting as auxiliary donors for Cu(I) coordination (Fig. 1). For example, the ligand PSP-1 offers an apparent dissociation constant of 0.8 fM and suffered no detectable oxidation upon continuous mixing with air for 15 d at 37 °C. PSP-2, which combines two PSP motifs in an EDTA-like architecture, is also air-stable and provides an even tighter K_d of 10 zM ($\log K = 20.04 \pm 0.06$), yet showed no evident interaction with Zn(II), Fe(II), or strong acid even at millimolar concentrations.

To harness the advantages of the PSP ligand design strategy within a Cu(I)-responsive fluorescent probe, we now report crisp-17 (Fig. 1), in which the electron-withdrawing PSP motif is incorporated into a push–pull fluorophore architecture (19) to yield an emission-ratiometric indicator suitable for two-photon excitation microscopy. Employed in live mammalian cells, crisp-17 allows visualization of base levels of labile Cu(I) as well as rapid dynamic changes evoked by treatment with the membrane-permeant thiosemicarbazone Cu(II) complex CuGTSM or the thiol-selective oxidant 2,2′-dithiodipyridine (DTDP). The experimental results reveal remarkably tight buffering in the low attomolar concentration range without evidence for significant participation of GSH under normal physiological conditions.

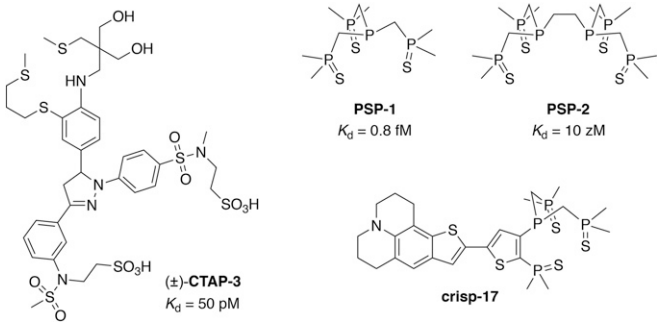

Fig. 1. Structure of the lipid-compatible fluorescent indicator CTAP-3 and Cu(I)-selective reagents utilizing phosphine sulfide-stabilized phosphine (PSP) coordination motifs, including ligands PSP-1 and PSP-2, and the Cu(I)-indicator crisp-17.

Results and Discussion

Cu(I) Is Rapidly Removed from CTAP-3 by Endogenous Ligands. To passively diffuse across the plasma membrane and reach cellular targets, fluorescent probes must be sufficiently lipophilic, a requirement that is often accompanied by poor water solubility, aggregation in aqueous solution, and accumulation in membranes or lipid droplets. These effects can produce large changes in fluorescence independently from the target analyte, making reliable interpretation of cellular staining patterns difficult if not impossible (20). Solubilized by two anionic sulfonate groups, CTAP-3 circumvents these effects to provide a high-contrast response to Cu(I) even in the presence of lipid bilayers (13). To probe to what extent endogenous ligands might remove Cu(I) from CTAP-3, we microinjected the preformed [Cu(I)–CTAP-3] complex (0.8 mM in 0.1 M KCl) into live BSC-1 cells (*SI Appendix*, Fig. S1). As the injection volume is estimated to be on the order of 10% compared with the total cell volume, the actual intracellular concentration is expected to be an order of magnitude lower. Even upon repeated injections, the fluorescence emission rapidly dissipated each time without evidence of saturation. To test whether this behavior could be explained by simple photobleaching, we doubled the time interval between each image acquisition. An overlay of the normalized decay profiles revealed a constant half-life near 15 s regardless of the frame rate (*SI Appendix*, Fig. S1*C*), confirming that the fluorescence decay corresponds to rapid demetallation of injected [Cu(I)-CTAP-3] by an endogenous ligand pool with large Cu(I) binding capacity. Our recently determined stability constants for the GSH–Cu(I) equilibrium system imply that normal cellular GSH levels alone could account for these results, regardless of the participation of other biomolecules (17). Imaging the availability of endogenous Cu(I) therefore requires a fluorescent probe with sufficient affinity to operate within and below the buffer window set by GSH, and we reasoned that our recently reported PSP ligand design strategy could be employed to meet this challenge.

Design and Synthesis of Crisp-17, an Emission-Ratiometric Cu(I)-Responsive Probe with Attomolar Dissociation Constant. Given the electron-withdrawing power of phosphine sulfide substituents, the PSP ligand motif can be readily integrated into a push–pull fluorophore architecture. Metal ion coordination would reinforce photoinduced intramolecular charge transfer (ICT), thus yielding a red shift of the absorption and emission spectra suitable for ratiometric imaging. As an added benefit, fluorophores with a large degree of ICT offer increased sensitivity for two-photon excitation microscopy, which minimizes background fluorescence, photobleaching, and phototoxicity. Aiming for a Cu(I) affinity intermediate between the tripodal monophosphine PSP-1 and diphosphine PSP-2, we replaced one of the methylene bridges of PSP-1 with a 2,3-disubstituted thiophene ring, which was combined with a thieno-fused julolidine heterocycle to provide strong charge donation.

The target probe crisp-17 (copper ratiometric indicator utilizing stabilized phosphines with stability constant $\log K = 17$; see below) was convergently assembled via building blocks **3**, **4**, and **6** (Fig. 2). Expedient access to the tetracyclic donor **3** was achieved via triple tandem cyclization of acetal **2** in refluxing 1-bromo-3-chloropropane. In this process, the hydrogen halides produced during formation of the julolidine ring system serve as acid catalysts for closure of the benzothiophene ring, while Hünig's base suppresses imine formation by delaying cleavage of the acetal until N-alkylation is complete. Final attachment of the phosphine sulfide-substituted phosphine moiety posed unexpected challenges: While PSP-1 and PSP-2 were obtained by substitution of phosphorus(III) electrophiles with lithiated trimethylphosphine sulfide, this approach proved incompatible with the dimethylphosphine sulfide group due to rapid proton exchange and subsequent intramolecular substitution. Taking advantage of the lower kinetic basicity of organomagnesium versus organolithium reagents, we

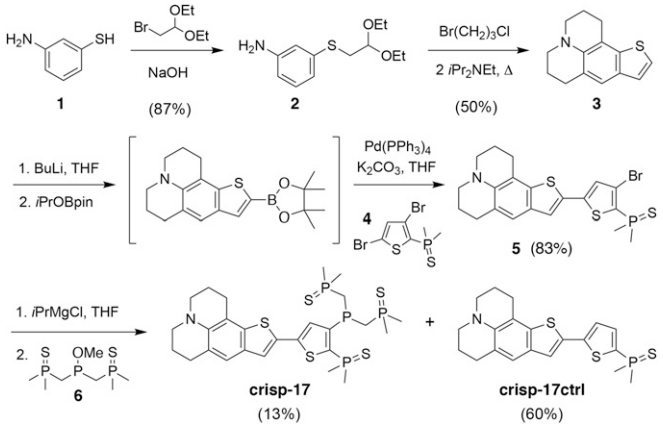

Fig. 2. Synthesis of the Cu(I)-responsive indicator crisp-17 and Cu(I)-insensitive control fluorophore crisp-17ctrl.

instead performed a magnesium-halogen exchange with intermediate **5** followed by substitution with phosphinite **6** to give crisp-17 product in 4.7% overall yield. The debrominated side product served as a control compound, crisp-17ctrl, which lacks the ability to chelate Cu(I).

Photophysical Characterization. To avoid potential interference from hydrophobic aggregation, we first characterized the Cu(I)-binding stoichiometry and fluorescence response of crisp-17 in 95% methanol–water. Molar ratio titration of crisp-17 with the low-affinity Cu(I) complex [Cu(I)MCL-2]PF_6 (21) revealed red shifts in absorption and emission maxima (Fig. 3 *A* and *B*), which were fully reversed upon addition of the high-affinity Cu(I) chelator PSP-2. Furthermore, the sharp saturation at 1 molar equivalent (Fig. 3 *B*, *Inset*) and clean isosbestic points in both absorption and emission spectra indicate a well-defined 1:1 Cu(I)-binding equilibrium. With these results at hand, we further characterized the probe in aqueous buffer in the presence of model lipid bilayers to evaluate its suitability for cellular imaging (19). Since cellular lipid bilayers comprise a variable mixture of neutral and anionic head groups, we prepared liposomes using a 4:1 ratio of zwitterionic palmitoyl oleoyl phosphatidylcholine (POPC) to anionic palmitoyl oleoyl phosphatidylglycerol (POPG) in aqueous buffer (13). After equilibration with the liposome mixture, crisp-17 gave a 65-nm shift in emission maximum from 555 to 620 nm upon saturation with Cu(I) (Fig. 3*C*) while remaining insensitive toward acidification (*SI Appendix*, Fig. S2). In contrast, crisp-17ctrl showed no spectral changes upon addition of [Cu(I)MCL-2]PF_6 (*SI Appendix*, Fig. S4). Although the fluorescence quantum yield of crisp-17 decreases from 55 to 21% upon Cu(I) complexation, the concomitant red shift in absorption (*SI Appendix*, Fig. S3) results in similar overall brightness for the free and Cu(I)-bound probe upon excitation at 450 nm (Fig. 3*C*) and thus a balanced spectral response well suited for ratiometric detection. For example, the ratio of fluorescence intensity from 590 to 750 nm versus 480–580 nm swings from 0.6 to 4 upon Cu(I)-saturation, yielding a sixfold dynamic range, while the presence of other first-row transition metal cations in fivefold excess over the probe has no effect (Fig. 3*D* and *SI Appendix*, Fig. S5).

To determine the apparent Cu(I)-binding affinity of crisp-17, we employed a saturated lipid mixture (4:1 DMPC–DMPG) to avoid possible interference from lipid peroxides. As shown in Fig. 4*A*, addition of 10 μM [Cu(I)MCL-1]PF_6 (K_d of 0.1 fM at μ = 0.1, 25 °C) (21) to 1 μM crisp-17 yielded a shift in emission maximum from 554 to 612 nm. Back-titration with excess MCL-1 followed by nonlinear least-squares fitting over the full wavelength range revealed an apparent affinity of log$K$ = 17.0 ± 0.1 (Fig. 4*B*), while a second titration employing 2 μM probe and 2.5 μM Cu(I) yielded log$K$ = 17.2 ± 0.1. The resulting mean affinity of log$K$ = 17.1 ± 0.1 (K_d of 8 aM) exceeds that of previous synthetic Cu(I) probes by four to six orders of magnitude and should be sufficient to measure Cu(I) availability in the presence of normal intracellular GSH levels. To confirm this prediction, we titrated 2 μM crisp-17 with Cu(I) in the presence of 4 mM GSH. At low Cu(I)/probe ratios, the fractional saturation of the probe indicated near-quantitative Cu(I)-binding, reaching 48% at 0.5 molar equivalents. At higher ratios, the onset of cooperative Cu(I)–GSH cluster assembly manifests as a clamping effect (17), which limited probe saturation to about 80% even at fivefold excess of Cu(I) (Fig. 4*C*). Thus, crisp-17 can indeed report Cu(I) availability both within and just below the GSH buffer window at typical cytosolic pH values (Fig. 4*D*). Furthermore, least-squares fitting using the stability constants for the Cu(I)–GSH equilibrium system (17) yielded an affinity of log$K$ = 17.1 ± 0.1 for crisp-17, thus independently confirming the above value.

Two-Photon Emission Ratiometric Imaging of Labile Cellular Cu(I). To examine the utility of crisp-17 as a ratiometric Cu(I) probe for two-photon excitation microscopy, we performed a series of imaging experiments with live NIH 3T3 mouse fibroblasts (Fig. 5). The adherent cells were grown in basal medium for 24 h followed by incubation with crisp-17 (1 μM) in serum-free medium for 20 min. With two-photon excitation at 880 nm, fluorescence micrographs were simultaneously collected over two emission channels of 479–536 nm (BP1) and 611–750 nm (BP2). As shown in Fig. 5*A*, crisp-17 readily entered cells and produced bright fluorescence staining throughout the cytoplasm. Areas of increased probe concentration appeared as distinct punctae, which were particularly apparent in the shorter wavelength channel (BP1). The corresponding intensity ratio image, obtained by dividing the integrated photon count for each pixel pair of the two channels (BP2/BP1), produced a rather uniform ratio distribution of 0.73 ± 0.2, with only small variations between individual cells. Notably, the bright punctae indicated a lower ratio compared with the cytosolic average, thus underscoring the

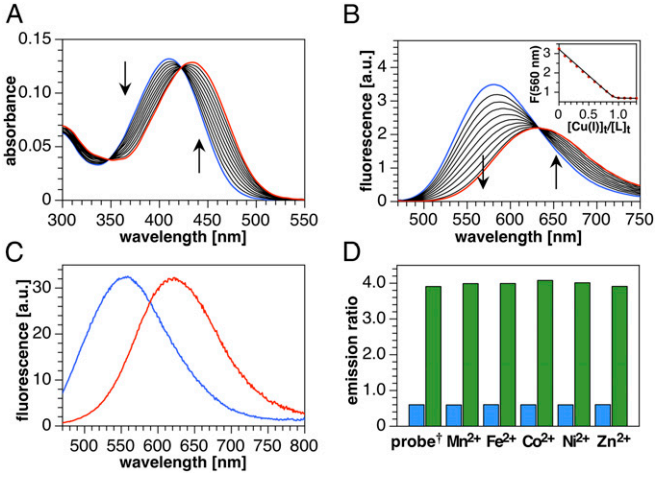

Fig. 3. Spectral response and selectivity of crisp-17 toward Cu(I) (supplied as [Cu(I)MCL-2]PF_6). (*A*) UV-vis absorption spectra of crisp-17 (5 μM) in 95% MeOH-5% H_2O during titration with Cu(I) (0–6.5 μM). (*B*) Fluorescence emission spectra (λ_{ex} = 460 nm) under the same conditions. (*Inset*) Emission intensity at 560 nm vs. molar ratio of Cu(I) to probe. (*C*) Emission spectra (λ_{ex} = 450 nm) of crisp-17 (2 μM) equilibrated with liposome suspension (4:1 POPC–POPG, 100 μM total lipids, 10 mM Pipes, pH 7.0, 0.1 M KCl, 25 °C) in the absence (blue trace) and presence (red trace) of 4 μM Cu(I). (*D*) Ratio of the integrated emission intensities *F*(590–750 nm)/*F*(480–580 nm) of crisp-17 (2 μM) in the presence of biologically relevant transition metal ions (10 μM) before (blue bars) and after (green bars) addition of 4 μM Cu(I) (liposome and buffer composition as in *C*). †Probe response in the absence of a competing metal ion.

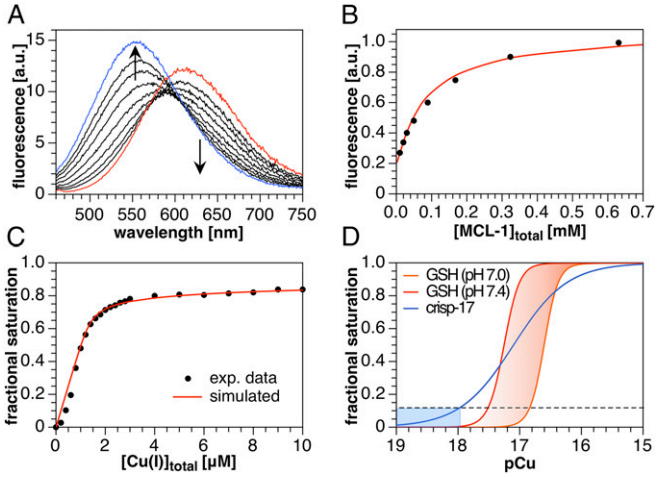

Fig. 4. Fluorimetric Cu(I) competition titrations of crisp-17 against MCL-1 and GSH (4:1 DMPC–DMPG, 100 μM total lipids, 10 mM Pipes, pH 7.0, 0.1 M KCl, 25 °C, λ_{ex} = 450 nm). (*A*) crisp-17 (1 μM) was equilibrated with 10 μM [Cu(I)MCL-1]PF_6 (red trace) at pH 7.0 and subsequently titrated with MCL-1 (10–640 μM, black traces). Full reversibility was confirmed by adding 10 μM PSP-2 (blue trace). Nonlinear least-squares fitting yielded log*K* of 17.0 ± 0.1. (*B*) Fit quality evaluated at 530 nm. (*C*) Apparent fractional saturation of crisp-17, calculated as $(I - I_{free})/(I_{bound} - I_{free})$, where *I* represents integrated fluorescence intensity from 500 to 550 nm, upon titration with Cu(I) (as [Cu(I)MCL-2]PF_6) in the presence of 4 mM GSH at pH 7.0. Least-squares fitting (red line) yielded log*K* = 17.1 ± 0.1. (*D*) Calculated fraction of crisp-17 bound to Cu(I) and of total Cu(I) bound to GSH versus thermodynamically available Cu(I) (pCu = $-\log[Cu^{+}_{aq}]$). The dashed line and blue shading demarcate the Cu(I) availability corresponding to 10% fractional saturation of the probe. The red-shaded area indicates the GSH Cu(I) buffer window within the cytosolic pH range.

benefit of ratiometric probes, which, unlike simple turn-on probes, compensate for uneven probe distributions.

To elicit a dynamic change in labile Cu(I), cells were exposed to CuGTSM, a lipophilic Cu(II) thiosemicarbazone complex that undergoes reduction ($E_{1/2}$ = −0.44 V vs. AgCl/Ag) upon cellular uptake followed by rapid dissociation of Cu(I) from the ligand (22, 23). In agreement with this mechanism, the cytoplasmic intensity ratio dramatically increased from 0.72 ± 0.04 (n = 20) to ∼1.00 ± 0.07 (Fig. 5*B*). Although higher ratios appear in cell nuclei, their significance is uncertain as the emission intensities in both channels are five to eight times lower compared with the cytoplasmic region. Similar distributions were observed with other lipophilic probes (10, 19) and presumably indicate a partition equilibrium that disfavors the polar nuclear environment. Addition of the membrane-permeant high-affinity Cu(I) chelator PSP-2 (50 μM) resulted in complete reversal of the initial change to reach an intensity ratio around 0.66 ± 0.05, slightly below the basal value (n = 20; P = 0.0008). In contrast to CuGTSM, the related Cu(II) thiosemicarbazone complex CuATSM yielded only a small increase of the intensity ratio (*SI Appendix*, Fig. S6), consistent with its more negative reduction potential ($E_{1/2}$ = −0.60 V vs. AgCl/Ag) (24), while a control experiment with crisp-17ctrl showed no ratio change upon exposure to CuGTSM (*SI Appendix*, Fig. S7). Although CuGTSM is toxic to cells (25, 26), an MTT assay revealed no toxicity for crisp-17 at up to 50 times the concentration employed for microscopy (*SI Appendix*, Fig. S8).

In a second set of experiments, we tested the ability of crisp-17 to respond to changes in endogenous copper availability. Mouse 3T3 fibroblasts incubated with crisp-17 showed a small, statistically nonsignificant increase of the fluorescence ratio from 0.65 ± 0.04 to 0.68 ± 0.05 (Fig. 5*C*; n = 20, P = 0.082) upon addition of the thiol-selective oxidant DTDP (27). Growing cells in medium supplemented with 50 μM $CuCl_2$ for 1 wk gave a negligible increase in the average ratio to 0.67 ± 0.03 (Fig. 5*D*) and no reduction in cell viability (*SI Appendix*, Fig. S8), despite the fact that the average total cellular copper levels increased more than twofold (*SI Appendix*, Fig. S11). However, treatment of these cells with DTDP produced a dramatic increase in fluorescence ratio up to 1.9 with an average of 1.12 ± 0.17 (n = 20) within the region of interest (ROI), consistent with dissociation of a sizable pool of Cu(I) from sulfhydryl coordination sites. A gradual regression of the ratio is also apparent, suggesting recapture of Cu(I) by endogenous ligands. Indeed, when

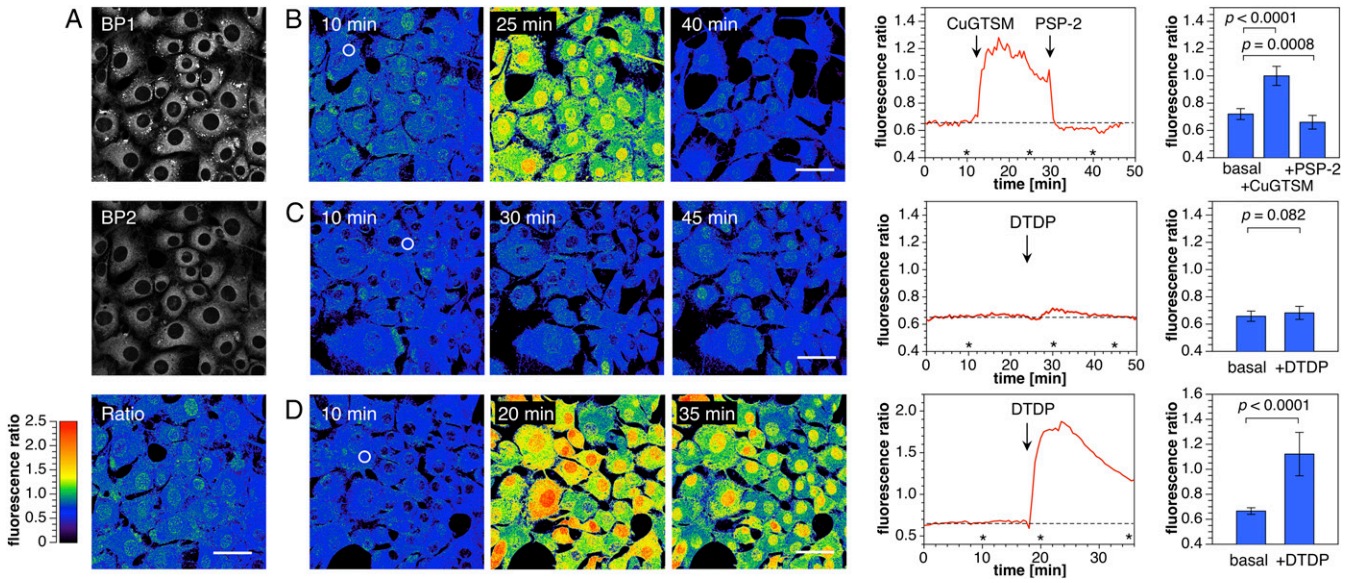

Fig. 5. Two-photon ratiometric imaging of labile copper dynamics in live mouse fibroblasts stained with crisp-17 (1 μM). (*A*, *Top*) Fluorescence intensity images acquired with emission channels of 479–536 nm (BP1) and 611–750 nm (BP2) with two-photon excitation at 880 nm. (*A*, *Bottom*) Ratio image with ratio = BP2/BP1. (*B*, *Left*) Ratio images before and after addition of 10 μM CuGTSM. (Scale bars, 50 μm.) (*B*, *Middle*) Time course of the average ratio change for the region of interest (ROI) indicated with a white circle in the *Left*. The asterisks indicate time points for the respective ratio images shown to the *Left*. (*B*, *Right*) Mean fluorescence ratio of the cytoplasmic region averaged over 20 cells (*P* values calculated for n = 20 using a two-tailed test). (*C*) Experiment as described for *B* but with addition of 1 mM 2,2′-dithiodipyridine (DTDP) in lieu of CuGTSM. (*D*) Experiment as described for *C* but employing cells grown in medium supplemented with 50 μM $CuCl_2$.

the experiment was repeated over a longer acquisition period, the ratio returned to the basal level after 80 min (*SI Appendix*, Fig. S9), a time frame that is sufficient for restoration of thiol-disulfide homeostasis after oxidative insult (28). Given that phosphines are frequently employed as disulfide-reducing agents, it is remarkable that the phosphine-based probe crisp-17 remains functional under conditions that rapidly liberate metals by oxidation of thiolate binding sites to disulfides (19). To confirm that the observed ratio changes are not due to a direct interaction of the probe with DTDP, we performed control experiments under acellular conditions. The fluorescence of 1 μM crisp-17 in 4:1 DMPC-DMPG liposome suspension was unaffected by direct exposure to 100 μM DTDP for 60 min (*SI Appendix*, Fig. S10*A*), whereas addition of DTDP in the presence of 2 μM purified copper-zinc metallothionein Cu_4Zn_4MT-2 (apparent $K_d = 0.4$ aM) (29) elicited a rapid spectral shift, reaching saturation within 30 min. Rapid reversal by PSP-2 (*SI Appendix*, Fig. S10*C*) confirmed that the response represents Cu(I) transfer. Considering that the average fluorescence ratio of crisp-17 is only around 0.72 under normal physiological conditions (Fig. 5*B*), we estimate that the fractional probe saturation is less than 12% (based on minimum and maximum ratios of 0.64 and at least 1.3, respectively). As indicated by the binding isotherm in Fig. 4*D*, this translates to a buffered Cu(I) concentration near 1 aM, just below the threshold for GSH–Cu(I) cluster assembly. Taken together, these results demonstrate that crisp-17 is suitable for dynamic monitoring of the thermodynamic availability of Cu(I) in live cells and indicate that, under normal physiological conditions, labile intracellular copper is not buffered directly by GSH but rather by endogenous ligands of still higher affinity.

Probing the Copper Phenotype of Menkes Fibroblasts. Menkes disease is an X-linked inherited disorder due to mutations of ATP7A, a copper-transporting P-type ATPase that localizes to the trans-Golgi network and delivers copper to cuproenzymes within the secretory pathway (30, 31). Although the disease leads to systemic copper deficiency due to impaired copper transport across enterocytes into the bloodstream, cultured fibroblasts from Menkes patients retain copper to a greater extent than normal cells due to impaired copper efflux (30, 31). To probe the impact of the compromised homeostatic system on intracellular copper availability, we performed a series of experiments with fibroblasts from two human pedigrees (Fig. 6*A*). Western blot analysis confirmed the absence of ATP7A in Menkes cells ($ATP7A^{-/y}$), whereas similar expression levels were observed in $ATP7A^{-/+}$ and normal $ATP7A^{+/y}$ cells (Fig. 6*B*). For two-photon imaging studies with crisp-17, cells were cultured in basal medium followed by supplementation with 50 μM $CuCl_2$ for 24 h. Consistent with the imaging data using 3T3 fibroblasts, all three cell lines yielded rather even ratio distributions throughout the cytoplasm (Fig. 6*C*). Although ATP7A-null cells accumulated over 10-fold higher copper compared with normal $ATP7A^{+/y}$ cells (Fig. 6*F* and *SI Appendix*, Fig. S11), the corresponding average fluorescence ratio was only slightly elevated from 0.63 to 0.70 (Fig. 6*G*). The low fractional saturation of crisp-17 indicates that ATP7A-null cells retain the ability to buffer copper within the low attomolar range, despite the large increase in total cellular copper. This observation is consistent with recent estimates of the Cu(I) binding affinity of metallothionein (29, 32), which is up-regulated in Menkes mutant cells and has been implicated as the major copper carrier (33). Although we found strong induction of metallothionein transcription in ATP7A-null cells as expected (*SI Appendix*, Fig. S12), no statistically significant changes were observed in copper-supplemented 3T3 cells for metallothionein or other proteins involved in copper homeostasis. These results suggest that metallothionein expression is preferentially up-regulated only under conditions of severe copper overload.

Despite strong buffering in ATP7A-null cells under basal conditions, the presence of elevated copper levels becomes clearly evident upon addition of DTDP, which induced a rapid

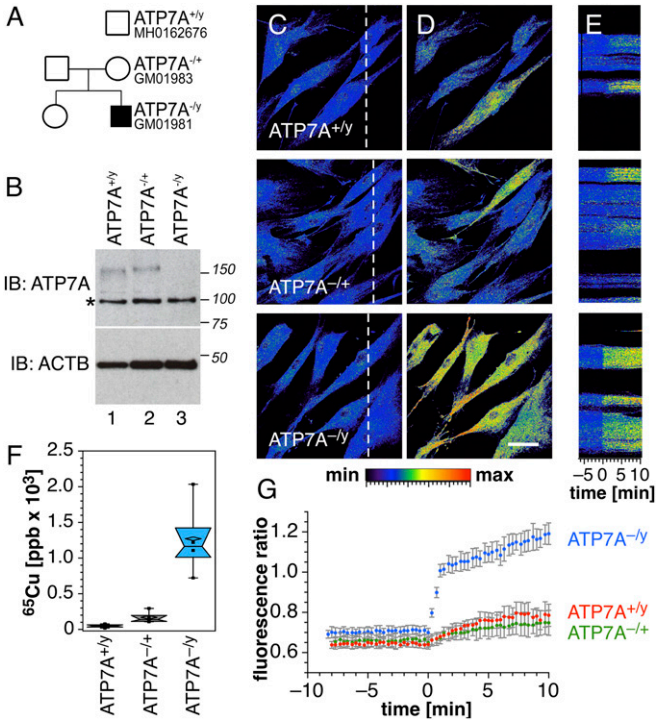

Fig. 6. Copper phenotypes of Menkes disease fibroblasts. (*A*) Pedigrees of a family affected by Menkes disease. (*B*) ATP7A-null subject GM01981 was confirmed by immunoblot analysis. Asterisk denotes nonspecific band recognized by the antibody. Loading controls were performed with anti–β-actin antibodies (ACTB). (*C*) Wild-type ($ATP7A^{+/y}$), carrier mother ($ATP7A^{-/+}$, GM01983), and Menkes son ($ATP7A^{-/y}$, GM01981) fibroblasts were imaged by two-photon microscopy with crisp-17. Color scale depicts copper-dependent emission ratio (0–2.5 range) at 570–640 nm/500–550 nm. (*D*) Copper was mobilized by the addition of the oxidizing reagent DTDP (100 μM). (Scale bar, 50 μm.) (*E*) Kymographs of cells in *C* (dashed line) with time 0 corresponding to the addition of DTDP. (*F*) Copper content phenotype confirmed by inductively coupled plasma mass spectrometry (one-way ANOVA followed by Dunnett's multiple comparisons; $n = 3$). (*G*) Fluorescence emission ratios before and after DTDP addition. Average ± SE from six independent experiments.

fluorescence ratio increase from 0.70 to 1.2 at 1/10th the dose applied in initial studies with 3T3 fibroblasts, while copper-supplemented $ATP7A^{-/+}$ and $ATP7A^{+/y}$ cells yielded only a small ratio increase (Fig. 6 *D* and *E*). Together, these studies demonstrate the utility of crisp-17 for characterizing phenotypes associated with defects in copper metabolism and confirm that living cells maintain tight buffering of available Cu(I) to the vicinity of 1 aM, even under conditions of impaired copper efflux.

In summary, we have developed a Cu(I)-selective ratiometric fluorescent probe, crisp-17, featuring a phosphine sulfide-stabilized phosphine (PSP) ligand architecture to achieve an apparent dissociation constant of 8 aM (log*K* 17.1), four to six orders of magnitude lower compared with previously reported synthetic Cu(I) probes (10–12). The probe features an appropriate combination of binding affinity, reversibility, sensitivity, and membrane permeability to permit dynamic monitoring of labile Cu(I) in live cells. On the basis of ratiometric imaging data, we demonstrate that, under normal physiological conditions, intracellular Cu(I) is buffered to the vicinity of 1 aM, which is below the threshold for cooperative assembly of GSH–Cu(I) clusters (17). Similar tight buffering was observed in cells characterized by elevated copper levels, for example in fibroblasts grown in Cu(II)-supplemented medium as well as Menkes mutant cells that suffer from impaired copper efflux. These results suggest that GSH does not serve directly as a Cu(I) reservoir, but rather plays an indirect role in copper homeostasis, for example

by controlling the redox state of Cu(I)-binding cysteine residues (34, 35). The activation of mammalian Cu/Zn superoxide dismutase (SOD1) in the absence of its metallochaperone CCS provides direct evidence for such a role. When cellular levels of oxidized GSH were increased through deletion of GSH reductase, the CCS-independent activation of SOD1 was abolished despite the fact that total GSH levels remained unaltered, thus suggesting delivery of copper by a yet-unidentified redox-sensitive carrier (36). While we do not exclude that direct buffering of Cu(I) by GSH may come to play under acutely toxic conditions, such as ionophore-mediated rapid influx of Cu(II) or partial oxidation of cellular thiols by DTDP, the ability of GSH–Cu(I) complexes to catalyze superoxide formation in vitro (37) implies that cellular Cu(I) levels should be maintained below the threshold for GSH cluster assembly to avoid toxicity in an oxygenated atmosphere. In contrast, the tetranuclear Cu(I)-cluster formed in the β-domain of metallothioneins is redox-inert in air (29), thus rendering metallothionein a safe Cu(I)-storage site, consistent with its up-regulation in ATP7A-null fibroblasts. Nevertheless, copper-supplemented 3T3 cells maintain tight control over Cu(I) availability without up-regulating metallothionein, thus suggesting the involvement of a more complex polydisperse buffer, potentially including yet-to-be-discovered thiol ligands. In light of this uncertainty, we prefer not to speculate as to the identity of the ligands involved.

As the sensing window of crisp-17 extends below the threshold of Cu(I) complexation by GSH, the probe should be well suited for monitoring transient changes of Cu(I), for example to screen potential copper-based metallodrugs or PET imaging agents for intracellular stability. Moreover, the remarkable redox stability of crisp-17 toward disulfides also enables studies of oxidatively mediated Cu(I) release, which would presumably be incompatible with the cysteine-based binding sites of genetically encoded Cu(I) probes (38). Given that the PSP ligand design strategy underpinning crisp-17 is capable of delivering still lower Cu(I) dissociation constants, we anticipate that this approach can be further tuned for maximal sensitivity toward endogenous changes in intracellular Cu(I) availability to study the interplay between cellular copper levels and other aspects of biology.

Materials and Methods

Detailed descriptions of all experimental methods are provided in *SI Appendix*, including the synthesis and characterization of crisp-17 and crisp-17ctrl, photophysical characterization, binding selectivity evaluation, binding affinity measurements, ratiometric two-photon imaging studies, and toxicity evaluation.

ACKNOWLEDGMENTS. Financial support from the National Institutes of Health (R01GM067169 to C.J.F., AG060285 to V.F., and R35GM12870 to G.M.) and the Robert A. Welch Foundation (AT-1935-20170325 to G.M.) is gratefully acknowledged.

1. H. Öhrvik, J. Aaseth, N. Horn, Orchestration of dynamic copper navigation—new and missing pieces. *Metallomics* **9**, 1204–1229 (2017).
2. S. Lutsenko, Human copper homeostasis: A network of interconnected pathways. *Curr. Opin. Chem. Biol.* **14**, 211–217 (2010).
3. N. J. Robinson, D. R. Winge, Copper metallochaperones. *Annu. Rev. Biochem.* **79**, 537–562 (2010).
4. S. M. Herd, J. Camakaris, R. Christofferson, P. Wookey, D. M. Danks, Uptake and efflux of copper-64 in Menkes'-disease and normal continuous lymphoid cell lines. *Biochem. J.* **247**, 341–347 (1987).
5. M. T. Morgan, P. Bagchi, C. J. Fahrni, "Fluorescent probes for monovalent copper" in *Metals in Cells*, Culotta V, Scott RA, Eds. (Wiley, 2013), pp. 65–84.
6. L. Banci, I. Bertini, K. S. McGreevy, A. Rosato, Molecular recognition in copper trafficking. *Nat. Prod. Rep.* **27**, 695–710 (2010).
7. A. Badarau, C. Dennison, Copper trafficking mechanism of CXXC-containing domains: Insight from the pH-dependence of their Cu(I) affinities. *J. Am. Chem. Soc.* **133**, 2983–2988 (2011).
8. A. M. Keller *et al*., Dynamic multibody protein interactions suggest versatile pathways for copper trafficking. *J. Am. Chem. Soc.* **134**, 8934–8943 (2012).
9. R. McRae, P. Bagchi, S. Sumalekshmy, C. J. Fahrni, In situ imaging of metals in cells and tissues. *Chem. Rev.* **109**, 4780–4827 (2009).
10. J. A. Cotruvo, Jr, A. T. Aron, K. M. Ramos-Torres, C. J. Chang, Synthetic fluorescent probes for studying copper in biological systems. *Chem. Soc. Rev.* **44**, 4400–4414 (2015).
11. C. J. Fahrni, Synthetic fluorescent probes for monovalent copper. *Curr. Opin. Chem. Biol.* **17**, 656–662 (2013).
12. C. Shen, E. J. New, What has fluorescent sensing told us about copper and brain malfunction? *Metallomics* **7**, 56–65 (2015).
13. M. T. Morgan, A. McCallum, C. J. Fahrni, Rational design of a water-soluble, lipid-compatible fluorescent probe for Cu(I) with sub-part-per-trillion sensitivity. *Chem. Sci. (Camb.)* **7**, 1468–1473 (2016).
14. J. H. Freedman, M. R. Ciriolo, J. Peisach, The role of glutathione in copper metabolism and toxicity. *J. Biol. Chem.* **264**, 5598–5605 (1989).
15. A. Bhattacharjee, K. Chakraborty, A. Shukla, Cellular copper homeostasis: Current concepts on its interplay with glutathione homeostasis and its implication in physiology and human diseases. *Metallomics* **9**, 1376–1388 (2017).
16. I. F. Scheiber, R. Dringen, Copper-treatment increases the cellular GSH content and accelerates GSH export from cultured rat astrocytes. *Neurosci. Lett.* **498**, 42–46 (2011).
17. M. T. Morgan, L. A. H. Nguyen, H. L. Hancock, C. J. Fahrni, Glutathione limits aqua-copper(I) to sub-femtomolar concentrations through cooperative assembly of a tetranuclear cluster. *J. Biol. Chem.* **292**, 21558–21567 (2017).
18. M. T. Morgan *et al*., Stabilization of aliphatic phosphines by auxiliary phosphine sulfides offers zeptomolar affinity and unprecedented selectivity for probing biological Cu^{I}. *Angew. Chem. Int. Ed. Engl.* **57**, 9711–9715 (2018).
19. D. Bourassa *et al*., Chromis-1, a ratiometric fluorescent probe optimized for two-photon microscopy reveals dynamic changes in labile Zn(II) in differentiating oligodendrocytes. *ACS Sens.* **3**, 458–467 (2018).
20. K. Price *et al*., The challenges of using a copper fluorescent sensor (CS1) to track intracellular distributions of copper in neuronal and glial cells. *Chem. Sci. (Camb.)* **3**, 2748–2759 (2012).
21. P. Bagchi, M. T. Morgan, J. Bacsa, C. J. Fahrni, Robust affinity standards for Cu(I) biochemistry. *J. Am. Chem. Soc.* **135**, 18549–18559 (2013).
22. P. S. Donnelly *et al*., An impaired mitochondrial electron transport chain increases retention of the hypoxia imaging agent diacetylbis(4-methylthiosemicarbazonato) $copper^{II}$. *Proc. Natl. Acad. Sci. U.S.A.* **109**, 47–52 (2012).
23. K. A. Price *et al*., Mechanisms controlling the cellular accumulation of copper bis(thiosemicarbazonato) complexes. *Inorg. Chem.* **50**, 9594–9605 (2011).
24. Z. Xiao, P. S. Donnelly, M. Zimmermann, A. G. Wedd, Transfer of copper between bis(thiosemicarbazone) ligands and intracellular copper-binding proteins. insights into mechanisms of copper uptake and hypoxia selectivity. *Inorg. Chem.* **47**, 4338–4347 (2008).
25. M. A. Cater *et al*., Increasing intracellular bioavailable copper selectively targets prostate cancer cells. *ACS Chem. Biol.* **8**, 1621–1631 (2013).
26. K. Y. Djoko *et al*., Copper(II)-bis(thiosemicarbazonato) complexes as antibacterial agents: Insights into their mode of action and potential as therapeutics. *Antimicrob. Agents Chemother.* **59**, 6444–6453 (2015).
27. E. Aizenman *et al*., Induction of neuronal apoptosis by thiol oxidation: Putative role of intracellular zinc release. *J. Neurochem.* **75**, 1878–1888 (2000).
28. K. Umezawa, M. Yoshida, M. Kamiya, T. Yamasoba, Y. Urano, Rational design of reversible fluorescent probes for live-cell imaging and quantification of fast glutathione dynamics. *Nat. Chem.* **9**, 279–286 (2017).
29. J. S. Calvo, V. M. Lopez, G. Meloni, Non-coordinative metal selectivity bias in human metallothioneins metal-thiolate clusters. *Metallomics* **10**, 1777–1791 (2018).
30. S. G. Kaler, ATP7A-related copper transport diseases-emerging concepts and future trends. *Nat. Rev. Neurol.* **7**, 15–29 (2011).
31. S. Zlatic, H. S. Comstra, A. Gokhale, M. J. Petris, V. Faundez, Molecular basis of neurodegeneration and neurodevelopmental defects in Menkes disease. *Neurobiol. Dis.* **81**, 154–161 (2015).
32. J. S. Scheller, G. W. Irvine, D. L. Wong, A. Hartwig, M. J. Stillman, Stepwise copper(I) binding to metallothionein: A mixed cooperative and non-cooperative mechanism for all 20 copper ions. *Metallomics* **9**, 447–462 (2017).
33. J. R. Riordan, L. Jolicoeur-Paquet, Metallothionein accumulation may account for intracellular copper retention in Menkes' disease. *J. Biol. Chem.* **257**, 4639–4645 (1982).
34. J. Brose, S. La Fontaine, A. G. Wedd, Z. Xiao, Redox sulfur chemistry of the copper chaperone Atox1 is regulated by the enzyme glutaredoxin 1, the reduction potential of the glutathione couple GSSG/2GSH and the availability of Cu(I). *Metallomics* **6**, 793–808 (2014).
35. W. C. J. Singleton *et al*., Role of glutaredoxin1 and glutathione in regulating the activity of the copper-transporting P-type ATPases, ATP7A and ATP7B. *J. Biol. Chem.* **285**, 27111–27121 (2010).
36. M. C. Carroll *et al*., Mechanisms for activating Cu- and Zn-containing superoxide dismutase in the absence of the CCS Cu chaperone. *Proc. Natl. Acad. Sci. U.S.A.* **101**, 5964–5969 (2004).
37. H. Speisky *et al*., Generation of superoxide radicals by copper-glutathione complexes: Redox-consequences associated with their interaction with reduced glutathione. *Bioorg. Med. Chem.* **17**, 1803–1810 (2009).
38. J. Liu, J. Karpus, S. V. Wegner, P. R. Chen, C. He, Genetically encoded copper(I) reporters with improved response for use in imaging. *J. Am. Chem. Soc.* **135**, 3144–3149 (2013).